S. Hinds, and R. Middleton, Nucl. Phys. A103, 33 (1967).

[21]R. Broglia, P. Federman, O. Hansen, K. Hehl, and C. Riedel, Nucl. Phys. A106, 421 (1968).

[22]R. Broglia and C. Riedel, Nucl. Phys. A92, 145 (1967).

[23]E. R. Flynn, R. Broglia, S. Landowne, B. Nilsson, and V. Paar, Nucl. Phys. (to be published).

[24]O. Hansen, in Proceedings of the International Conference on Properties of Nuclear States, Montréal,

Canada, 1969, edited by M. Harvey et al. (Presses de l'Université de Montréal, Montréal, Canada, 1969), p. 421.

[25]J. B. Ball, R. L. Auble, J. Rapaport, and C. B. Fulmer, Phys. Letters 30B, 533 (1969).

[26]B. Sørensen, Nucl. Phys. (to be published).

[27]J. Ball, R. Auble, and P. Roos, Phys. Rev. C 4, 196 (1971).

# Elastic Scattering of $^{16}$O by $^{56}$Fe, $^{70,74}$Ge, and $^{90}$Zr[†]

A. W. Obst, D. L. McShan, and R. H. Davis

*Department of Physics, The Florida State University, Tallahassee, Florida 32306*

(Received 2 August 1972)

The elastic scattering of $^{16}$O by $^{56}$Fe, $^{70}$Ge, $^{74}$Ge, and $^{90}$Zr has been studied in the vicinity of the Coulomb barrier for the purpose of extracting optical-model parameters and barrier heights. Angular distributions were measured from 30° to 170° in the lab in 10° steps and in the bombarding energy range from 30 to 60 MeV in 2-MeV steps. No discrete ambiguities in the real potentials were found, probably due to the large imaginary potentials. Barrier heights determined with the optical-model parameters were found to be consistent with Greiner's calculated barrier heights and 10–20% lower than the ordinary Coulomb barrier $Z_1 Z_2 e^2/1.35(A_1^{1/3} + A_2^{1/3})$.

## I. INTRODUCTION

Credible predictions of the barrier height, the energy at which two nuclear masses just touch, are important to the design of future experiments with very heavy ions. In the adiabatic approximation model used by Beringer,[1] the two colliding masses become oblate with respect to a common axis, with the result that the interaction barrier is significantly raised above that for two spheres. Greiner[2] and others[3,4] have predicted barriers by solving the time-dependent collision problem, in which the collision time and the characteristic oscillation periods of the individual nuclei are related. For oscillation periods longer than the collision time, the nuclei do not have time to align themselves preferentially and the barrier is lowered. Oscillation periods shorter than the collision time are more difficult to excite, but once excited can also reduce the barrier by the periodic extension of the nuclei towards one another. It is, furthermore, not clear to what extent the nuclear diffuseness affects the above considerations.[3]

The two most straightforward methods of measuring the height of the barrier are optical-model analysis of elastic scattering and the onset of reactions. Systematic data of either type are scarce for heavy ions.[5] A third possible means of establishing the barrier is in the interference minima

in inelastic heavy-ion scattering.[6] However, until these can be sufficiently well correlated with theory, a precise determination of the barrier this way is difficult.

In the present work optical-model analysis of elastic scattering was used to find barrier heights for $^{16}$O on several medium-weight nuclei from $^{40}$Ca to $^{120}$Sn. These are compared with the classical values and also with the predictions of the dynamic models. The results for Ni are compared to available ($^{16}$O, $xn$) and ($^{16}$O, $xp$) measurements.

## II. EXPERIMENTAL METHOD

The Florida State University super FN tandem Van de Graaff was used to produce a beam of 30- to 60-MeV $^{16}$O ions of charge states 5 or 6. Fifteen point angular distributions were measured in 2-MeV steps using 15 Si surface-barrier detectors mounted in a ring at 10° intervals from 30 to 170° in the lab. The over-all energy resolution was about 300–500 keV, as seen in Fig. 1.

Also seen in Fig. 1 are the first-excited-state 2$^+$ groups in $^{56}$Fe (0.845 MeV), $^{70}$Ge (1.04 MeV), $^{74}$Ge (0.596 MeV), and $^{90}$Zr (2.18 MeV); the second 2$^+$ state groups in $^{74}$Ge (1.20 MeV); the third 2$^+$ state in $^{90}$Zr (3.84 MeV); and the first 3$^-$ state group in $^{90}$Zr (2.74 MeV). At the forward angles these excited-state groups are barely discernible

above the background from the large elastic
groups, while at the backward angles they become
comparable in magnitude to the elastic groups.
Oxygen peaks were seen at the forward angles,
since the targets consisted of oxides evaporated
onto carbon backings, except for $^{90}$Zr, which was
an evaporated foil.

Absolute cross sections were obtained by mea-
suring simultaneously $^{16}$O elastic scattering from
a thin flash of gold evaporated onto the targets.
Up to 60 MeV, $^{197}$Au($^{16}$O, $^{16}$O) scattering obeys
Rutherford's law. The ratio of gold to sample tar-
get thicknesses was obtained at the lowest bom-
barding energies (~30 MeV), since here the scat-
tering from both sample and gold is Coulomb. Af-
ter each excitation function measurement the 30-
MeV runs were repeated to check target stability.

The relative errors on the data, including peak
fitting errors where applicable, ranged from ±4%
at the forward angles to ±80% at the backward an-
gles, just before the peaks became lost in the back-
ground with increasing angle and energy. The ab-
solute normalization error was about ±2%.

## III. ANALYSIS AND RESULTS

Angular distributions of the elastic scattering of
$^{16}$O on $^{56}$Fe, $^{70}$Ge, $^{74}$Ge, and $^{90}$Zr are shown in
Figs. 2-5. The solid curves represent optical-
model fits using the computer code JIB[7] with a
Woods-Saxon real and imaginary potential. Exten-
sive three- and four-parameter searches were
carried out for the real and imaginary well depths
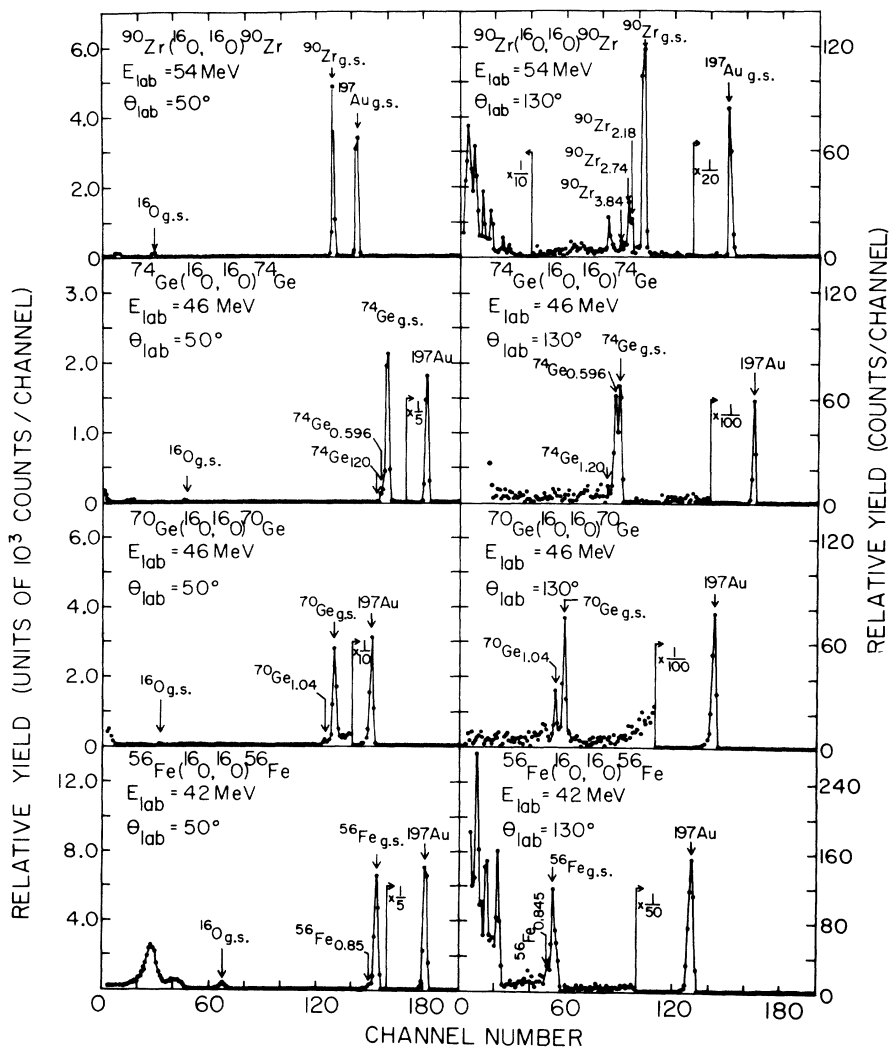$U$ and $W$ and the geometry parameters $r_0$ and $a$,



FIG. 1. Experimental energy spectra for $^{16}$O on $^{56}$Fe, $^{70}$Ge, $^{74}$Ge, and $^{90}$Zr.

where $R = r_0(A_1^{1/3} + A_2^{1/3})$ and $a$ is the diffuseness. The geometry parameters $r_0$ and $a$ were then fixed at the best average values ($r_0 = 1.25$ fm, $a = 0.6$ fm except for $^{90}$Zr, where $a = 0.5$ fm), and two-parameter searches were performed for $U$ and $W$. The smaller value of $a$ for $^{90}$Zr might reflect a more spherical closed-shell nucleus.

The falloff of the measured cross sections from the Rutherford cross sections is more rapid for the heavier isotope $^{74}$Ge than for the lighter isotope $^{70}$Ge. This same behavior was observed for $^{16}$O scattering from the even isotopes of Ni (Ref. 8), and is probably related to the larger reaction cross section due to the neutron excess. In some cases the data fall noticeably above the optical-model fits at the backward angles.
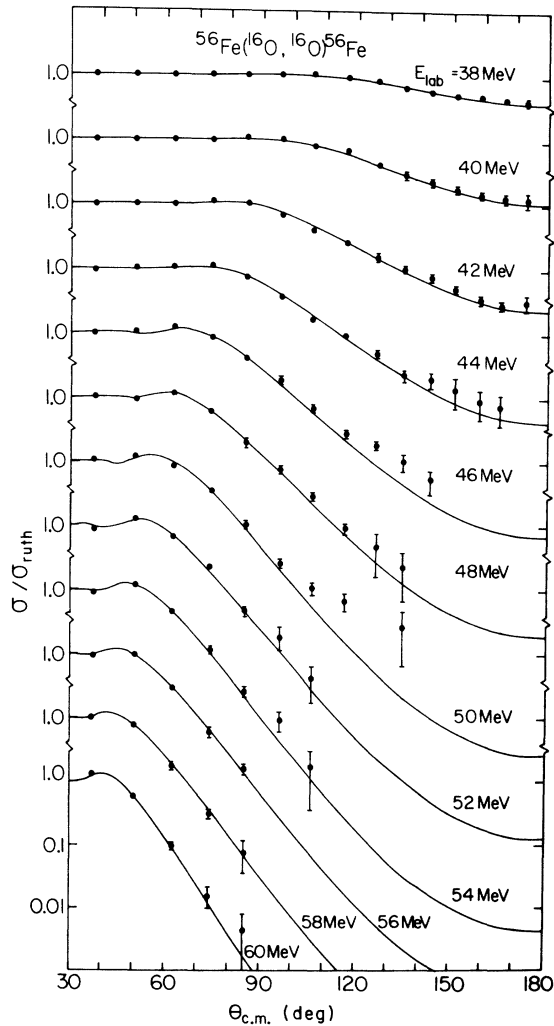
Since most of the reaction cross section in this range of mass and energy seems to be due to light outgoing particles,[9] it might be expected from angular momentum conservation requirements that the imaginary part of the potential be $l$-dependent.[10, 11] The inclusion of $l$ dependence, however, introduced large oscillations in the calculations at backward angles, which were not present in the data.

A compound-nuclear contribution to the data was estimated from the statistical model[12] with the simplification given by Eberhard *et al.*,[13] where the sum over all exit channels into which the compound nucleus can decay is replaced by an explicit expression obtained from the Fermi-gas model. In this approximation, Eq. (19) of Ref. 13, the parameters appearing in the sum over exit channels are the density of spin-zero states in the com-
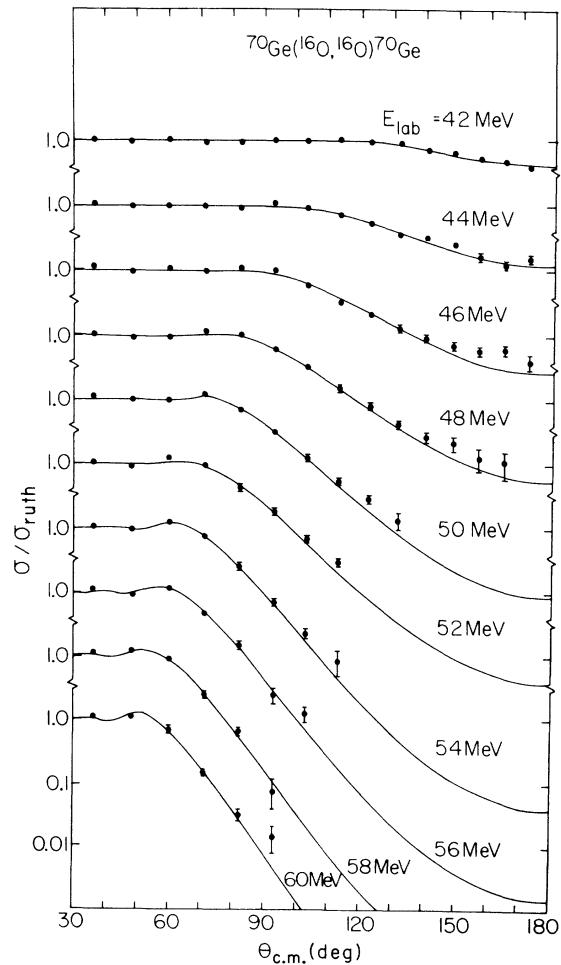


FIG. 2. Experimental angular distributions for $^{56}$Fe- $(^{16}$O$,^{16}$O$)^{56}$Fe at 38–60 MeV. The solid lines are optical-model fits (see text).



FIG. 3. Experimental angular distributions for $^{70}$Ge- $(^{16}$O$,^{16}$O$)^{70}$Ge at 42–60 MeV. The solid lines are optical-model fits (see text).

pound nucleus $(\rho = \Gamma_0/D_0)$ and an average value of the spin distribution parameter $(\sigma)$ for the various residual nuclei reached by the decay of the compound nucleus. The parameters $\rho$ and $\sigma$ were evaluated assuming only single-nucleon emission of neutrons, protons, and $\alpha$ particles, which in view of the work of Robinson, Kim, and Ford[9] is certainly an oversimplification. The derived cross sections were, in all cases except $^{56}$Fe, several orders of magnitude smaller than the shape elastic scattering. If the normalization is raised to equal the experimental cross section around 90°, then the calculated compound cross sections, which rise backwards of 90°, would lie well above the data, which decreases drastically at the backward angles.

The best-fit real and imaginary potentials are shown in Figs. 6–9 as a function of bombarding energy. Uncertainties on the parameters were obtained from $\chi^2 + 1$ contours in the $U$-$W$ plane. A straight-line fit was made through each of the four

real potential sets $U$, and the results are presented in Table I. The best-fit values of $W$ corresponding to this linearly varying $U$ did not deviate appreciably from the values of $W$ shown. Except for a few low-energy points on the $^{74}$Ge $U$-$W$ plot (Fig. 8), the absorption can be seen to increase from zero and level off with increasing bombarding energy. The arrows on Figs. 6–9 represent the Coulomb barrier as discussed below.

No type I or discrete ambiguities were found, as can be seen in Fig. 10. The region of $U$ space was explored beyond 1000 MeV, although the ordinate here extends only to 800 MeV. A unique value of $U$ is in fact to be expected due to the large absorption, as shown in the recent work of Watson, Robson, Tolbert, and Davis.[14]

As expected, there was some evidence of the continuous $Ur^n$ ambiguity from four-parameter searches, although in most cases the radius parameter $r_0$ did not deviate significantly from 1.25 fm. Another continuous ambiguity of the form[15]

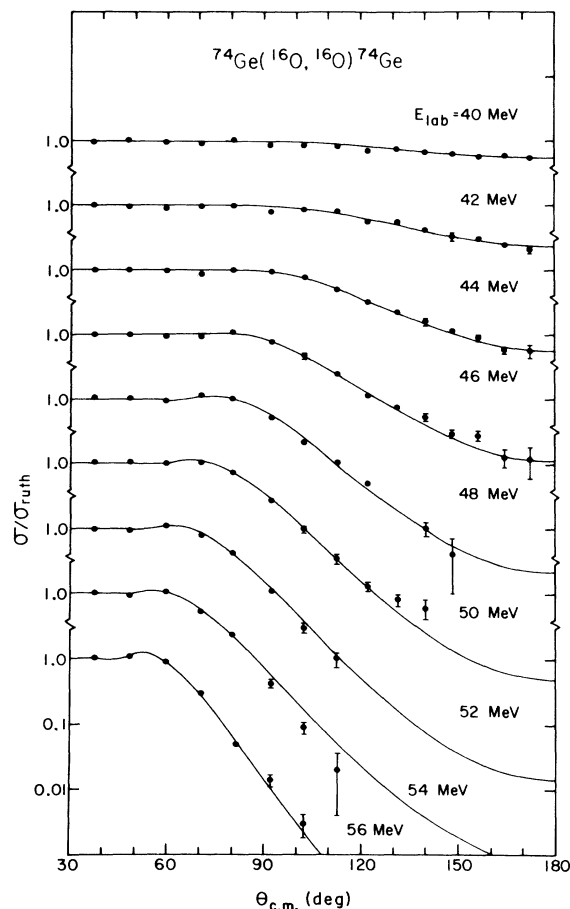$$Ue^{(R_N - R_B)/a} = \text{const} \qquad (1)$$



FIG. 4. Experimental angular distributions for $^{74}$Ge-$(^{16}$O,$^{16}$O$)^{74}$Ge at 40–56 MeV. The solid lines are optical-model fits (see text).
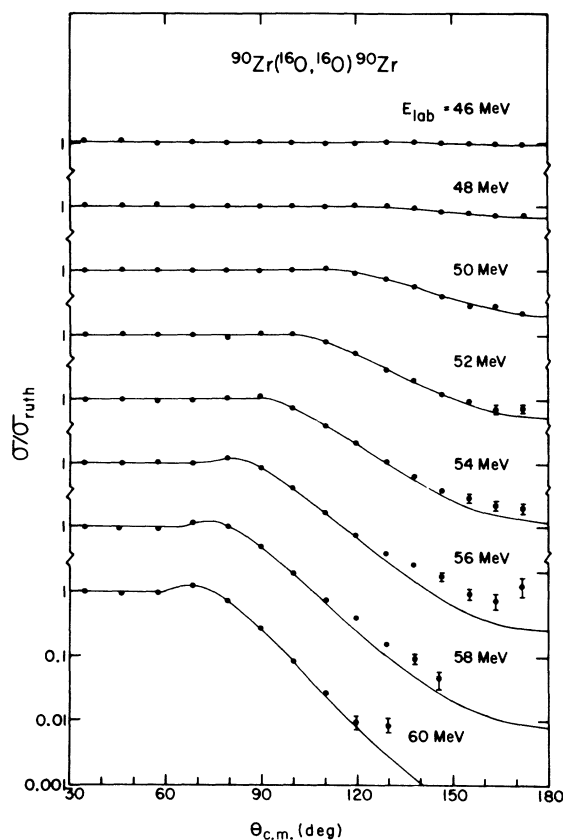
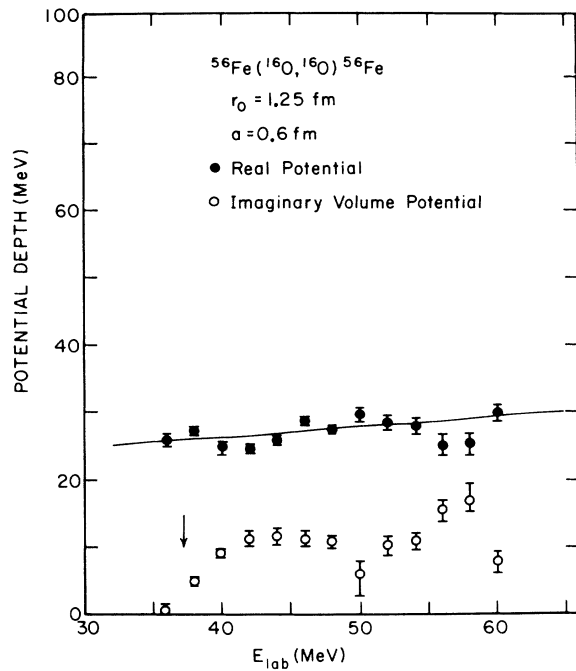FIG. 5. Experimental angular distributions for $^{90}$Zr-$(^{16}$O,$^{16}$O$)^{90}$Zr at 46–60 MeV. The solid lines are optical-model fits (see text).

FIG. 6. The real and imaginary optical potentials for
$^{56}$Fe($^{16}$O, $^{16}$O)$^{56}$Fe. A straight-line fit to the real potential
is shown. The arrow indicates the barrier energy deter-
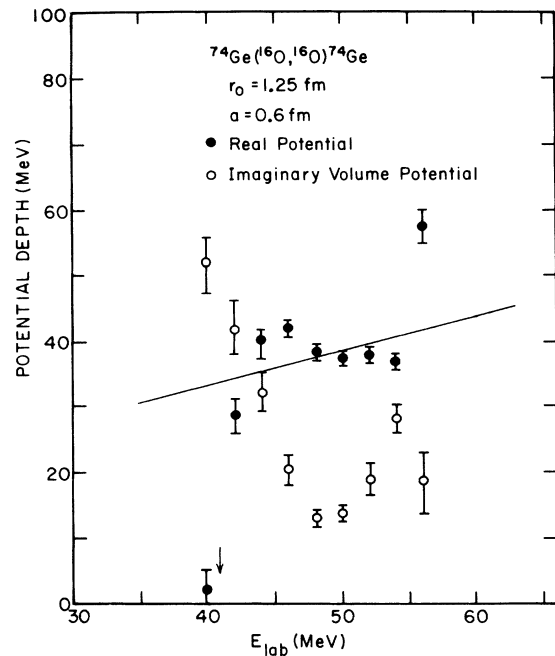mined from the real potential.



FIG. 8. The real and imaginary optical potentials for
$^{74}$Ge($^{16}$O, $^{16}$O)$^{74}$Ge. A straight-line fit to the real potential
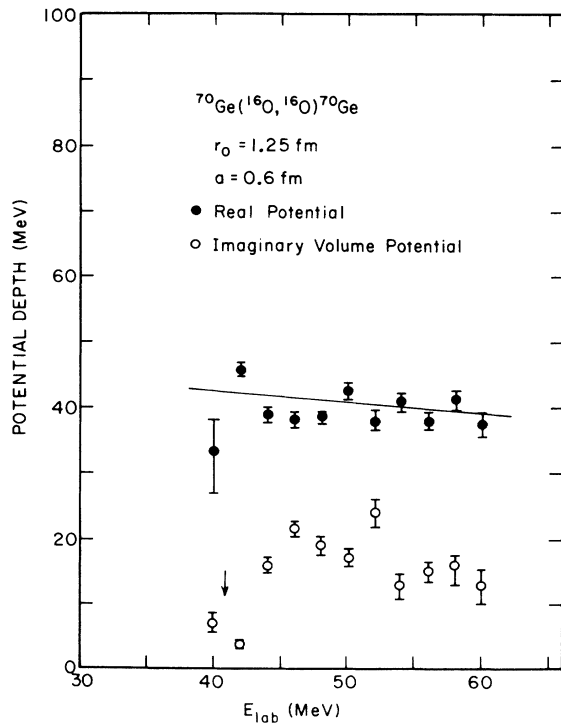is shown. The arrow indicates the barrier energy deter-
mined from the real potential.



FIG. 7. The real and imaginary optical potentials for
$^{70}$Ge($^{16}$O, $^{16}$O)$^{70}$Ge. A straight-line fit to the real potential
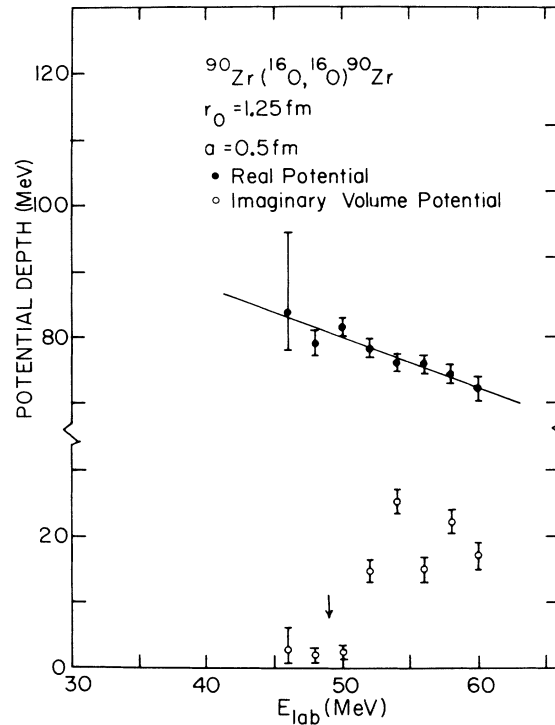is shown. The arrow indicates the barrier energy deter-
mined from the real potential.



FIG. 9. The real and imaginary optical potentials for
$^{90}$Zr($^{16}$O, $^{16}$O)$^{90}$Zr. A straight-line fit to the real potential
is shown. The arrow indicates the barrier energy deter-
mined from the real potential.

was also observed. Here $R_N$ is the nuclear radius, $R_B$ is the radius of the barrier defined by the maximum in the Coulomb+nuclear potential, and $a$ is the diffuseness. The locus of $\chi^2$ minima from three-parameter fits can be seen in Fig. 11 for $^{16}$O+$^{74}$Ge at 10 bombarding energies which label the points. The same result [Eq. (1)] is presented in Fig. 12 to show the linear relationship of $\ln(U)$ vs $1/a$ more clearly. The barrier $V_B$ can be written as

$$V_B = V_C(R_B) + \frac{U}{1+e^{(R_B-R_N)/a}},\qquad (2)$$

where $V_C$ is the Coulomb potential. Since
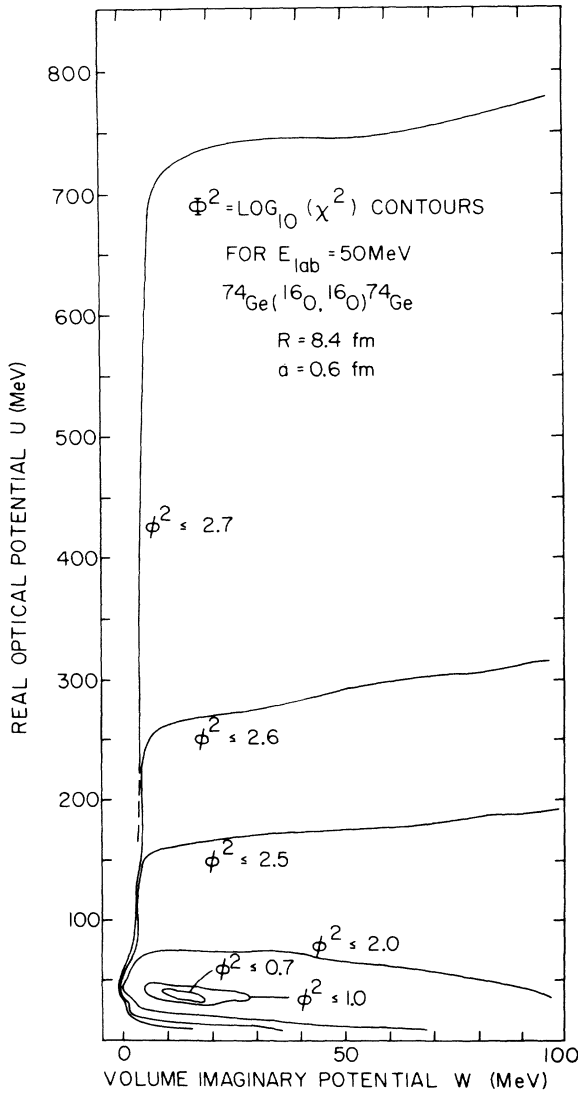
$$e^{(R_B-R_N)/a} \gg 1 \qquad (3)$$

TABLE I. Linear fit $U = U_0 + \Delta U x E_{lab}$ for $^{16}$O scattering in the energy range 30 MeV$\leq E_{lab} \leq 60$ MeV.

| Target | $U_0$ | $\Delta U$ |
|--------|-------|------------|
| $^{56}$Fe | $19.8 \pm 1.7$ | $0.16 \pm 0.04$ |
| $^{70}$Ge | $50.3 \pm 3.0$ | $-0.20 \pm 0.06$ |
| $^{74}$Ge | $12.6 \pm 5.7$ | $0.52 \pm 0.11$ |
| $^{90}$Zr | $117.5 \pm 7.8$ | $-0.75 \pm 0.14$ |

for $a < 1$ fm, we then have

$$\ln(U) \simeq \frac{1}{a}(R_B - R_N) + \ln(V_B - V_C). \qquad (4)$$

Here $R_B$ and $V_B$ are approximately constant for a given projectile and target, as shown below, and therefore we have a linear relationship between $\ln(U)$ and $1/a$. For a given $R_N$, then, only the three parameters $U$, $W$, and $a$ are needed to describe the scattering.

The barrier heights for each of the four targets studied are shown in Fig. 13 and also by the arrows in Figs. 6–9. The standard deviation on these barriers, determined from the scatter for different bombarding energies, is only about $\pm 300$ keV. This result is not unexpected, since the barrier is situated some distance from the nuclear surface. Also presented in Fig. 13 are the $^{40}$Ca data of Bertin et al.,[16] the $^{48}$Ti data of Orloff and Daehnick,[17] the Ni data of Fletcher and West,[8] and the Sn data of Robertson et al.[18] The "ordinary" Coulomb barrier is defined here as $Z_1 Z_2 e^2 / R$, with $R = 1.35(A_1^{1/3} + A_2^{1/3})$ for $A < 100$ and $R = 1.2(A_1^{1/3} + A_2^{1/3})$ for $A > 100$.[19] The calculations of Greiner and Holm,[2] which include only quadrupole and octupole vibrations, are seen to agree well with all of
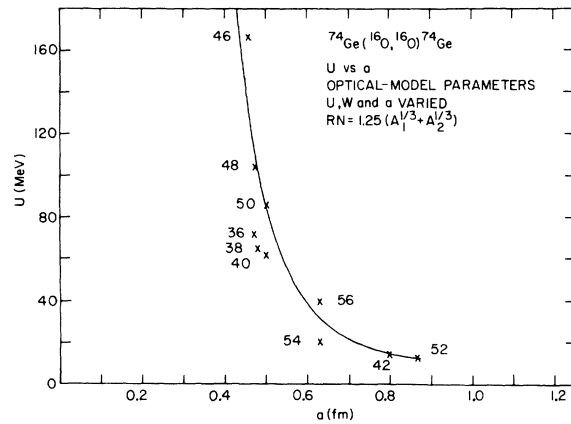
FIG. 10. Contours of constant $\chi^2$ in the $U$-$W$ plane showing a unique solution for $U$.

FIG. 11. The continuous $U$-$a$ ambiguity for $^{74}$Ge-$(^{16}$O, $^{16}$O$)^{74}$Ge. The solid curve was drawn to aid the eye. The numbers on the graph correspond to the locations of the best-fit $U$-$a$ combinations at different bombarding energies.
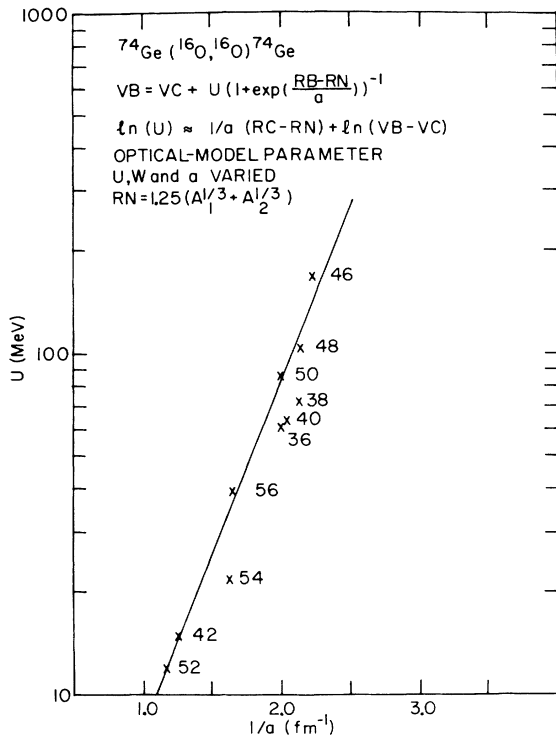
FIG. 12. The continuous $U$-$a$ ambiguity for $^{74}$Ge-$(^{16}O,^{16}O)^{74}$Ge. The solid line was drawn through the best-fit $\ln(U)$ vs $1/a$ points at the different bombarding energies to emphasize the $Ue^{r/a}$ ambiguity.



FIG. 13. The experimental barrier heights (●) presented along with the ordinary Coulomb barrier (×) given by $Z_1 Z_2 e^2/R$ (see text), and the dynamic calculations of Holm and Greiner (○) and Jensen and Wong (+).

the data, as far as the magnitude of the departure from the classical barrier is concerned. Some recent calculations of Jensen and Wong[4] are also shown, and these lie 1–2 MeV below the data.

The barrier height determined from the onset of the $(^{16}O, xn)$ and $(^{16}O, xp)$ reactions on $^{58}$Ni by Robinson, Kim, and Ford $(V_B = 29.1 \text{ MeV})$ (Ref. 9) is in good agreement with the present optical-potential analysis of the scattering data $(V_B = 30.8 \text{ MeV})$. In fact, for all the targets studied except $^{74}$Ge the rise of $W$ in Figs. 6–9 is in good agreement with the barrier heights, as indicated by the arrows.

## IV. CONCLUSION

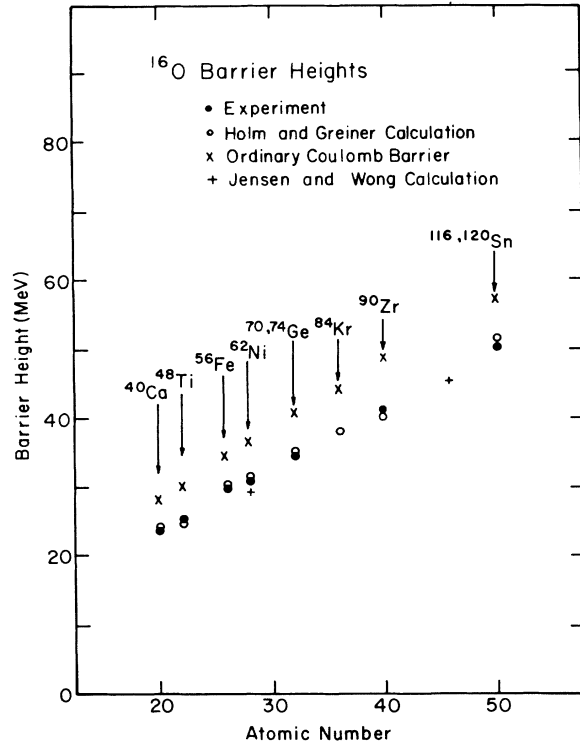The present study has demonstrated the accuracy of the classical dynamic predictions[2] and also

the applicability of the optical model to the study of heavy-ion interactions. A simple inclusion of $l$ dependence or compound-nuclear contribution does not remove the disagreement of some of the calculations with the data at the backward angles. The erratic behavior of $W$ with $E$, also seen in the work of Orloff and Daehnick,[17] indicates the need for some extensions of the optical model for heavy-ion scattering, although this behavior may in fact reflect coupling to reaction channels.

[1]R. Beringer, Phys. Rev. Letters **18**, 1006 (1967).
[2]H. Holm and W. Greiner, Phys. Rev. Letters **24**, 404 (1970).
[3]P. W. Riesenfeldt and T. D. Thomas, Phys. Rev. C **2**,

2448 (1970).

[4]A. S. Jensen and C. Y. Wong, Nucl. Phys. A171, 1 (1971).

[5]H. Gauvin, Y. Le Beyec, M. Lefort, and C. Deprun, Phys. Rev. Letters 28, 697 (1972).

[6]F. Videbaek, I. Chernov, P. R. Christensen, and E. E. Gross, Phys. Rev. Letters 28, 1072 (1972).

[7]F. G. Perey, Phys. Rev. 131, 745 (1963). An integration step length of 0.1 fm provided sufficient accuracy, as checked with the program LENS II.

[8]N. R. Fletcher, L. West, and K. W. Kemper, Bull. Am. Phys. Soc. 16, 1149 (1971).

[9]R. L. Robinson, H. J. Kim, and J. L. C. Ford, Bull. Am. Phys. Soc. 17, 531 (1972).

[10]A. E. Bisson and R. H. Davis, Phys. Rev. Letters 22, 542 (1969).

[11]R. A. Chatwin, J. S. Eck, D. Robson, and A. Richter, Phys. Rev. C 1, 795 (1970).

[12]H. Feshbach, Nuclear Spectroscopy (Academic, New York, 1960), Part B, p. 625.

[13]K. A. Eberhard, P. Von Brentano, M. Böhning, and R. O. Stephen, Nucl. Phys. A125, 673 (1969).

[14]B. D. Watson, D. Robson, D. D. Tolbert, and R. H. Davis, Phys. Rev. C 4, 2240 (1971).

[15]G. Igo, Phys. Rev. Letters 1, 72 (1958); Phys. Rev. 115, 1665 (1959).

[16]M. C. Bertin, S. L. Tabor, B. A. Watson, Y. Eisen, and G. Goldring, Nucl. Phys. A167, 216 (1971).

[17]J. Orloff and W. W. Daehnick, Phys. Rev. C 3, 430 (1971).

[18]B. C. Robertson, J. T. Sample, D. R. Goosman, K. Nagatani, and K. W. Jones, Phys. Rev. C 4, 2176 (1971).

[19]H. Holm, private communication.

---

# Fission of $^{234}$U and $^{236}$U with 14.8-MeV Neutrons*

D. R. Nethaway and B. Mendoza

*University of California, Lawrence Livermore Laboratory, Livermore, California 94550*

(Received 23 June 1972)

We determined mass-yield distributions from fission of $^{234}$U and $^{236}$U with 14.8-MeV neutrons. We measured the yields of 24 products covering the mass range 66–161 for $^{234}$U and for 30 products covering the mass range 66–172 for $^{236}$U. We estimated total chain yields by correcting for the effects of nuclear-charge dispersion in fission. The mass-yield curves are similar to those for fission of $^{233}$U, $^{235}$U, and $^{238}$U with 14.8-MeV neutrons. We measured the independent fractional chain yields of the following nuclides: for $^{234}$U: $^{96}$Nb, $(1.54 \pm 0.10) \times 10^{-3}$; $^{136}$Cs, $0.095 \pm 0.006$; for $^{236}$U: $^{96}$Nb, $(2.7 \pm 0.3) \times 10^{-4}$; $^{126}$Sb, $0.096 \pm 0.010$; $^{136}$Cs, $0.022 \pm 0.002$.

## INTRODUCTION

In this study of the mass-yield distribution for fission of $^{234}$U and $^{236}$U with 14.8-MeV neutrons, the $^{234}$U products that were measured ranged from $^{66}$Ni to $^{161}$Tb and, for $^{236}$U, from $^{66}$Ni to $^{172}$Er. No previous measurements have been reported for fission of these isotopes with 14-MeV neutrons. These measurements are part of a series that include $^{235}$U and $^{238}$U fission[1] and $^{233}$U fission[2] with 14-MeV neutrons. This paper deals specifically with $^{234}$U and $^{236}$U; we reported elsewhere[3] on a detailed examination of the fission distribution for all five uranium isotopes. The $^{234}$U measurements were made as relative yields and then converted to absolute fission yields by adjusting the total area under each half of the mass-yield curve to unity. The $^{236}$U calculations are based both on that method and on the measurement of the number of fissions.

## EXPERIMENTAL DETAILS

Our experimental details are similar to those reported previously[1,2] and are described here only briefly. The 14.8-MeV neutron irradiations were made at the insulated-core-transformer (ICT) accelerator at the Lawrence Livermore Laboratory. The uranium targets were placed at 0° to the source of neutrons produced by the reaction of a 400-keV deuteron beam on a rotating titanium tritide target. The 14-MeV D-T neutron source strength was typically $1 \times 10^{12}$ sec$^{-1}$ or greater; the flux density in the uranium target was about $2 \times 10^{10}$ cm$^{-2}$sec$^{-1}$, with very little decrease, if any, during an 8-h irradiation.

The $^{234}$U target assembly consisted of about 48 mg U$_3$O$_8$ (99.33% $^{234}$U, with $<5 \times 10^{-4}$% $^{233}$U, 0.36% $^{235}$U, 0.11% $^{236}$U, and 0.20% $^{238}$U) wrapped in aluminum foil and sealed in a thin polyethylene bag. The assembly was placed in a 30-mil cadmium